Real-Time Impedance-Based Stability Assessment of Grid Converter Interactions

Tuomas Messo, Roni Luhtala, Tomi Roinila
Tampere University of Technology
Laboratory of Electrical Energy Engineering
Tampere, Finland
tuomas.messo@tut.fi

Dongsheng Yang, Xiongfei Wang, Frede Blaabjerg
Aalborg University
Department of Energy Technology
Aalborg, Denmark
doy@et.aau.dk

***Abstract*—This paper proposes a method to monitor the impedance-based stability margin of grid-connected converters in real-time. A three-phase converter is configured to inject a broadband perturbation on top of its nominal output current to enable online identification of grid impedance. The ratio of converter and grid impedance is computed in real-time by utilizing the measured grid impedance and the analytical impedance model of the inverter. A Nyquist contour is plotted based on the impedance ratio. The contour can be used to assess impedance-based stability margin and to allow, e.g., adaptive tuning, more efficient post-fault diagnostics or to enable re-selection of control parameters. The method is implemented on a dSPACE real-time control platform and the associated Control Desk software. The paper also discusses potential limitations and suggests future improvements. A short video is available online to further illustrate the method.**

Keywords— impedance-based stability analysis, online grid impedance measurement, pseudo-random binary sequences, grid-connected three-phase inverter

I. INTRODUCTION

Power quality and stability problems in grid-connected power electronics, such as photovoltaic and wind power inverters have become a serious concern in the field of power electronics. A photovoltaic power plant was recently reported to suffer from unexplained instability problems characterized by distortions, which can vary within a wide frequency-range [1]. Stability of wind power plant has been shown to be compromised when the power converters interact with a series compensated line [2].

It is clear that power electronics and power engineering communities are facing profound problems, which have to be solved to allow large-scale integration of renewable energy sources, since these power generation systems are commonly interfaced by using power electronics converters. The reported harmonic resonance phenomenon can severely impact the rate at which the share of renewable energy is increased in the near future. Therefore, tools and methods to identify and mitigate the resonance phenomenon should be developed.

Interaction between the inverter and the equivalent grid impedance (as seen by the power converter) has been identified as one of the most likely causes for the reported stability and power quality problems. However, power electronics converters still lack the necessary diagnostic tools to identify the presence of impedance-related instability. The output currents and voltages can be monitored and recorded to facilitate post-fault diagnostics, as has been done in [1]. However, the reason for instability may be hard to identify based on current and voltage waveforms alone. In this paper, an impedance-based analysis is proposed to enable more informative monitoring and diagnostics, since the stability margin can be directly visualized from the ratio of the grid and inverter impedances [3].

Stability is preserved if the inverter impedance is shaped to have a larger magnitude than grid impedance at all frequencies or if both the grid and inverter impedance remain passive [4]. That is, the real parts of both impedances remain positive at all frequencies. However, the grid impedance varies over time and may experience multiple resonances [5], which makes impedance design of grid-connected converter a challenging task. Moreover, the inverter impedance is affected by control delays and necessary control functions, such as grid synchronization, which may introduce negative resistance-like behavior [6],[7]. A small stability margin may cause poorly damped oscillations in grid current and voltage during faults and transients, whereas, zero or negative stability margin causes instability and elevated harmonic, sub-harmonic and inter-harmonic currents [8].

In this paper an online stability analysis method is proposed. The method is implemented within the control system of grid-connected converter without the need of additional sensors. Extensive research in the field of online stability analysis has been carried out previously in [9]–[11]. However, the method in [9] relies on vector-fitting algorithm and in [10], an inductive grid impedance is assumed. In our work, the measured grid impedance is used directly and, thus, no assumptions about the impedance shape are required. Moreover, the proposed method does not require additional measurement equipment as demonstrated in [12].

The proposed method is based on injection of a pseudo-random-binary-sequence signal (PRBS). The PRBS is a wideband perturbation with controllable frequency resolution and power spectrum. Moreover, the maximum amplitude of the PRBS signal can easily be controlled. The PRBS was previously

demonstrated to be suitable for online grid impedance measurement in [13].

The proposed method calculates the ratio of grid and inverter impedance online based on measured grid impedance and the inverter impedance model. The model includes current control, active damping and grid voltage feedforward loops with the associated control delays. It is shown that the method can be effectively used to visualize the impedance-based stability margin, which allows the impedance-based interactions to be distinguished from other types of faults. The method is also able to visualize the Nyquist contour even under severe instability. Therefore, post-fault monitoring after inverter shut-down becomes possible. The proposed method provides a promising alternative to identify and mitigate resonance issues associated with grid-connected converters. Moreover, the method provides an attractive platform in the field of adaptive control algorithms for future research.

II. Real-Time Stability Assessment

A. Impedance-based stability criterion

Fig. 1 depicts the equivalent small-signal circuit of a three-phase output-current-controlled inverter in a non-ideal grid. Impedance-based stability margin can be evaluated by considering the multivariable root-loci derived from the return-ratio matrix $\mathbf{Z}_{\text{grid}}\left(\mathbf{Z}_{\text{inv}}\right)^{-1}$ and by applying the generalized Nyquist stability criterion. The impedances are defined in the dq-domain as given in (1) and (2).

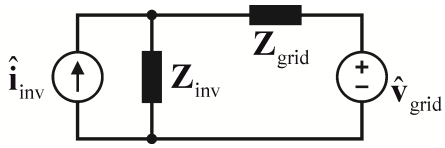

Fig. 1: Equivalent small-signal circuit model of grid-connected inverter.

$$\mathbf{Z}_{\text{grid}} = \begin{bmatrix} Z_{\text{dd-grid}} & Z_{\text{qd-grid}} \\ Z_{\text{dq-grid}} & Z_{\text{qq-grid}} \end{bmatrix} \tag{1}$$

$$\mathbf{Z}_{\text{inv}} = \begin{bmatrix} Z_{\text{dd-inv}} & Z_{\text{qd-inv}} \\ Z_{\text{dq-inv}} & Z_{\text{qq-inv}} \end{bmatrix} \tag{2}$$

It is common to approximate the stability criterion by assuming negligible off-diagonal impedances. It should be noted that stability analysis may produce erroneous results in the case of significant cross-couplings [14]. However, for the purpose of real-time implementation, the stability criterion should be as simple as possible in order to avoid significant computational burden. To reduce the complexity, stability is visually evaluated from the ratio of impedance d-components, i.e., the impedance ratio is considered as $Z_{\text{dd-grid}} / Z_{\text{dd-inv}}$. Stability analysis regarding the q-components is considered as a part of future research since simultaneous measurement of both d and q-components is required and, therefore, two uncorrelated injection signals should be injected to the grid currents [15].

The real-time stability assessment method requires online measurement of the grid impedance d-component $Z_{\text{dd-grid}}$ and an accurate, but yet, simple analytical model for the inverter impedance d-component $Z_{\text{dd-inv}}$. It should be noted that the work presents a first attempt for real-time stability analysis based on grid impedance measurement and an analytical impedance model. Therefore, the simplifications regarding the impedance model and stability criterion are considered acceptable.

B. Inverter impedance model

A three-phase inverter with LCL-filter and the associated control system is illustrated in Fig. 2. Active damping is used, which is derived from the three-phase capacitor voltage by using a high-pass filter G_{ad}. The d-component of three-phase capacitor voltage, v_{Cfd}, is used as feedforward variable in order to reject background harmonics in the grid voltage [16]. Current control is implemented in the dq-domain and a conventional phase-locked-loop is used. Moreover, the capacitor voltage and inverter-side inductor currents are used to identify the d-component of grid impedance from the ratio $v_{\text{Cfd}} / i_{\text{L1d}}$. Thus, additional sensors are not required.

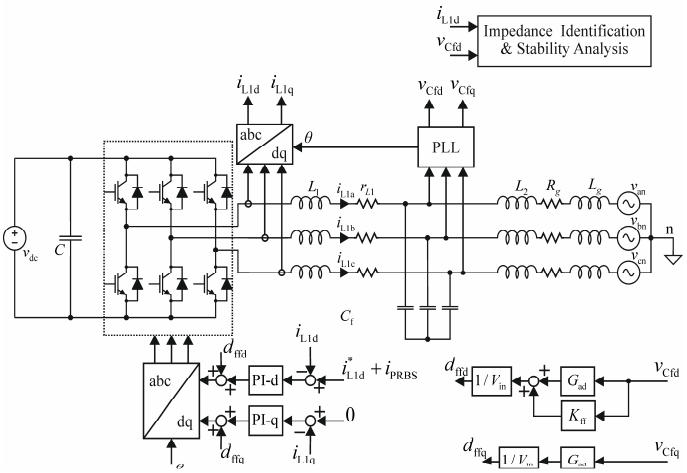

Fig. 2: Three-phase grid-connected inverter with its control.

All the measured feedback and feedforward variables should be taken at the interface at which the impedance-based stability is evaluated. Moreover, the inverter impedance model should be as simple as possible to reduce computational burden. To make the implementation of the method possible using the existing equipment, the output capacitors and grid-side inductors are considered as a part of the grid impedance according to Fig. 3. Therefore, the grid impedance includes a parallel resonance, but the inverter impedance model can be significantly simplified, as it can be analyzed by considering a simple L-type output filter. The inverter and controller parameters are collected in Table I.

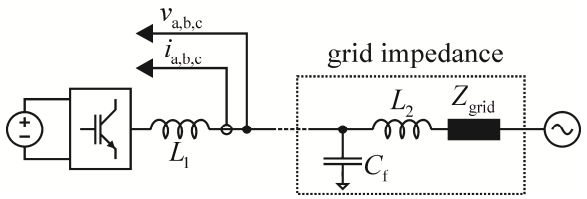

Fig. 3: Simplification of inverter impedance model.

Table I: Inverter and controller parameters.

V_{dc}	730 V	L_1	1.5 mH	K_P	0.012
$V_{g\text{-rms}}$	230 V	C_f	4 μF	K_I	17.9
f_{grid}	50 Hz	L_2	0 / 1.5 / 5 / 6.5 mH	K_{AD}	1.7
f_{sw}	10 kHz	i^*_{L1d}	5 A	ω_{AD}	$2\pi\cdot$5kHz
r_{L1}	100 mΩ	i^*_{L1q}	0 A	K_{ff}	0…1

According to Fig. 3, the inverter can be considered with pure L-type output filter, which greatly simplifies the analytical impedance model. Moreover, additional sensors are not required for grid impedance measurement since the three-phase voltage $v_{a,b,c}$ and current $i_{a,b,c}$ represent the input voltage and current of the grid impedance. The grid impedance can be measured simply as the ratio of d-components v_{Cfd} and i_{L1d}.

The perturbation, which is required for impedance measurement, is added in the reference of inverter output current, e.g., the d-component i^*_{L1d}, to extract grid impedance d-component. Likewise, the grid impedance q-component can be measured by injecting the perturbation to current q-component i^*_{L1q}. However, analysis related to the impedance q-component is out of the scope of this paper and will be considered in future research.

A three-phase inverter with an L-type filter can be represented around its steady-state operating point using a set of linearized state matrices as in (3), where D_d and D_q represent the steady-state duty ratio in the dq-domain and I_{Ld} and I_{Lq} represent the steady-state inductor currents in the dq-domain.

$$\frac{\mathrm{d}}{\mathrm{d}t}\mathbf{x}=\overbrace{\begin{bmatrix}-\frac{r_{L1}}{L_1} & \omega_s\\ -\omega_s & -\frac{r_{L1}}{L_1}\end{bmatrix}}^{\mathbf{A}}\mathbf{x}+\overbrace{\begin{bmatrix}\frac{D_d}{L_1} & -\frac{1}{L_1} & 0 & \frac{V_{in}}{L_1} & 0\\ \frac{D_q}{L_1} & 0 & -\frac{1}{L_1} & 0 & \frac{V_{in}}{L_1}\end{bmatrix}}^{\mathbf{B}}\mathbf{u}$$
$$\mathbf{y}=\overbrace{\begin{bmatrix}\frac{3D_d}{2} & \frac{3D_q}{2}\\ 1 & 0\\ 0 & 1\end{bmatrix}}^{\mathbf{C}}\mathbf{x}+\overbrace{\begin{bmatrix}0 & 0 & 0 & \frac{3I_{Ld}}{2} & \frac{3I_{Lq}}{2}\\ 0 & 0 & 0 & 0 & 0\\ 0 & 0 & 0 & 0 & 0\end{bmatrix}}^{\mathbf{D}}\mathbf{u} \quad (3)$$

The transfer matrix between inputs **u** and outputs **y** can be solved in the frequency-domain according to (4) and the transfer functions can be collected from the resulting transfer matrix **G** as shown in (5). The transfer functions are not given in a symbolic form due to page limitation. However, an example m-file is provided in the Appendix to solve the transfer functions using MATLAB.

$$\mathbf{G}=\mathbf{C}\left(s\mathbf{I}-\mathbf{A}\right)^{-1}\mathbf{B}+\mathbf{D} \quad (4)$$

$$\overbrace{\begin{bmatrix}\hat{i}_{in}\\ \hat{i}_{L1d}\\ \hat{i}_{L1q}\end{bmatrix}}^{\mathbf{y}}=\overbrace{\begin{bmatrix}Y_{in\text{-}o} & T_{oid\text{-}o} & T_{oiq\text{-}o} & G_{cid\text{-}o} & G_{ciq\text{-}o}\\ G_{iod\text{-}o} & -Y_{odd\text{-}o} & -Y_{oqd\text{-}o} & G_{codd\text{-}o} & G_{coqd\text{-}o}\\ G_{ioq\text{-}o} & -Y_{odq\text{-}o} & -Y_{oqq\text{-}o} & G_{codq\text{-}o} & G_{coqq\text{-}o}\end{bmatrix}}^{\mathbf{G}}\overbrace{\begin{bmatrix}\hat{v}_{in}\\ \hat{v}_{cfd}\\ \hat{v}_{cfq}\\ \hat{d}_d\\ \hat{d}_q\end{bmatrix}}^{\mathbf{u}} \quad (5)$$

The control block diagram, which represents the d-channel output dynamics, can be depicted as shown in Fig. 4 when the cross-coupling transfer functions $Y_{oqd\text{-}o}$ and $G_{coqd\text{-}o}$ are neglected. The subscript '-o' denotes the transfer functions are open-loop transfer functions, i.e., they are not affected by control loops. The reader is advised to see [14], [17] and for further details.

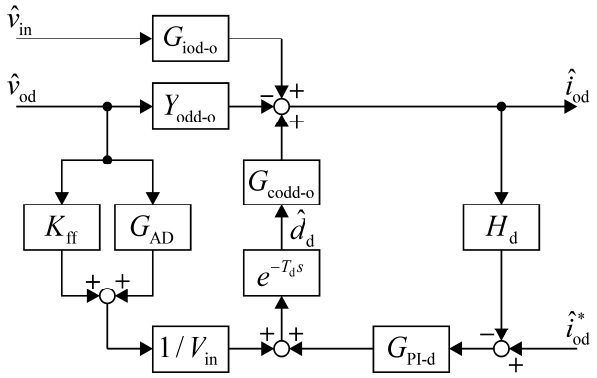

Fig. 4: Reduced-order block diagram from which admittance d-component $Z_{dd\text{-}inv}$ is solved.

Closed-loop output impedance can be solved from the block diagram of Fig. 4 and given as

$$Z_{dd\text{-}inv}(s)=-\frac{\hat{v}_{Cfd}}{\hat{i}_{L1d}}=\frac{1+G_{PI}(s)G_{codd\text{-}o}(s)G_{del}(s)}{Y_{odd\text{-}o}(s)-G_{codd\text{-}o}(s)\frac{1}{V_{in}}\left(K_{ff}+G_{ad}(s)\right)G_{del}(s)}, \quad (6)$$

where $G_{PI}=K_P+K_I/s$ is the current controller transfer function, $G_{ad}=K_{ad}s/\left(s+\omega_{ad}\right)$ is the active damping transfer function and K_{ff} is the proportional gain of the grid voltage feedforward loop. The open-loop transfer functions, $G_{codd\text{-}o}$ and $Y_{odd\text{-}o}$ can be approximated as given in (7) and (8), when the cross-coupling effect caused by the Park's transformation (or ω_s) is neglected. The cross-couplings affect mainly the low-frequency dynamics.

$$Y_{\text{odd-o}} = \frac{1}{r_{\text{L1}} + L_1 s} \tag{7}$$

$$G_{\text{codd-o}} = \frac{V_{\text{in}}}{r_{\text{L1}} + L_1 s} \tag{8}$$

The closed-loop inverter output impedance d-component can be solved from (6) and given symbolically as in (9) where the delay T_{del} is defined as 1.5 times the switching period.

$$Z_{\text{dd-inv}} = \frac{r_{\text{L}} + Ls + \left(K_{\text{P}} + \dfrac{K_{\text{I}}}{s}\right) V_{\text{in}} e^{-T_{\text{del}} s}}{1 - \left(K_{\text{ff}} + \dfrac{K_{\text{ad}} s}{s + \omega_{\text{ad}}}\right) e^{-T_{\text{del}} s}}. \tag{9}$$

The impedance can be solved in the frequency-domain (as a frequency response) by substituting the Laplace variable s with $j\omega$ where ω corresponds to a frequency vector. Moreover, the impedance can be computed online using a pre-determined frequency vector, to enable real-time stability analysis. In principle, the frequency-response of the inverter impedance in (9) is computed every time the grid impedance is measured and the Nyquist contour is plotted. Moreover, the delay can be computed as

$$e^{-j\omega T_{\text{d}}} = \cos\left(\omega T_{\text{d}}\right) - j\sin\left(\omega T_{\text{d}}\right). \tag{10}$$

Figs. 5 and 6 show the inverter impedance d-component extracted from a switching model (Simulink/ SimPowerSystems) as the red curve. The impedance measurement equipment were not available during the writing of this paper and, therefore, the impedance model is verified using a simulator instead. The blue curve is the approximated impedance according to (9) and the green dotted line represents the corresponding frequency response data extracted from the dSPACE control platform. The approximated transfer function corresponds to the simulated impedance fairly well. Thus, the analytical model can be used in real-time stability analysis. However, it should be noted that the deviation in phase and gain around one kilohertz might impose accuracy errors in the computed Nyquist contour. However, a different hardware should be used in the future to enable using a more complex impedance model to improve the accuracy.

It is evident from Fig. 6 that the impedance becomes non-passive with the nominal feedforward gain, i.e., $K_{\text{ff}} = 1$. That is the case when the phase is less than – 90 degrees over a wide frequency range and, thus, indicating a negative real part.

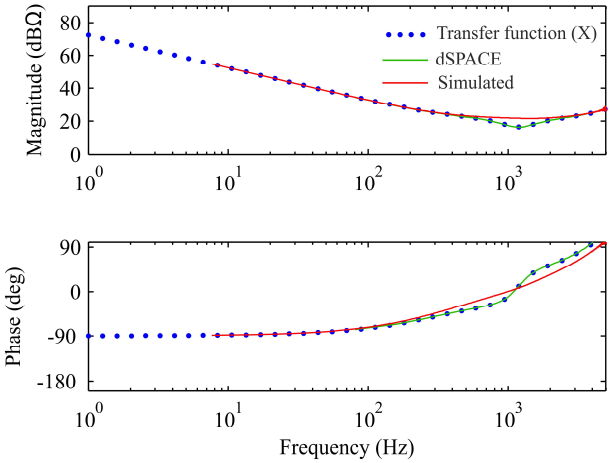

Fig. 5: Inverter impedance d-component with 50% feedforward gain.

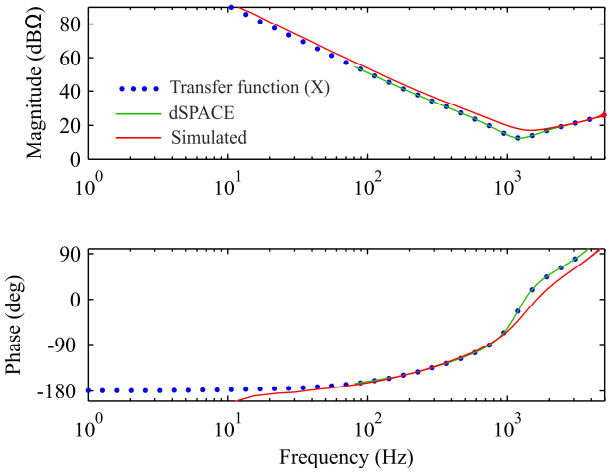

Fig. 6: Inverter impedance d-component with 100% feedforward gain.

C. Grid impedance measurement method

This paper applies pseudo-random binary sequence (PRBS) for obtaining the grid impedance. The PRBS is a periodic broadband excitation with the following key properties:

1) The signal has two levels, and it can switch the level only at certain event points $t = 0, \Delta t, 2\Delta t, \ldots$
2) The PRBS is deterministic and experiments are repeatable.
3) The sequence is periodic with period $T = N\Delta t$, where N is an odd integer.
4) Within one period, there are $(N+1)/2$ intervals when the signal is at one level and $(N-1)/2$ intervals when it is at the other

A PRBS is based on a sequence of length N. The most commonly used signals are based on maximum-length sequences (MLBS). Such sequences exists for $N = 2^n - 1$ where n is an integer. The reason for their popularity is that they

can be generated using a feedback shift register circuit, as shown in Fig. 7.

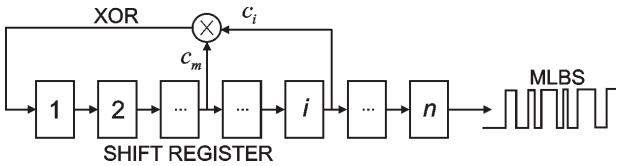

Fig. 7: *n*-bit shift register used for perturbation.

Fig. 8 shows the form of the power spectrum of the MLBS. The sequence is generated using a 4-bit-long shift register at 10 kHz and has signal levels ± 1V. The power spectrum has an envelope and drops to zero at the generation frequency and its harmonics. The generation frequency is one of the design variables of the sequence. The injection frequency must be high enough to cover the measurable frequency band.

The MLBS is well suited for sensitive systems that require small-amplitude perturbation. The signal has the lowest possible peak factor, which means that the signal does not present large peaks (compared e.g. to sum of sinusoids). Because the MLBS is deterministic, it can be repeated and injected precisely and the signal-to-noise ratio can be increased by synchronous averaging of the response periods.

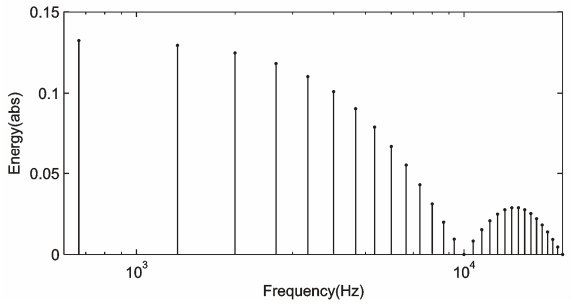

Fig. 8: Power spectrum of 15-bit-length MLBS generated at 10 kHz.

The grid impedance d-component is measured by injecting a PRBS signal on top of the grid current reference value i^*_{L1d}. The PRBS signal is generated using a five-bit shift register. The generation frequency of MLBS is 10 kHz, which is essentially the same as the inverter switching frequency. The measured grid current and voltage waveforms are sampled with 2.5 kHz frequency. The measurement is computed as the ratio of Fourier-transformed grid current and voltage d-components according to (11). A detailed discussion on the PRBS method can be found in [18].

$$Z_{\text{dd-grid}}(\mathrm{j}\omega) = \frac{\mathbf{V}_{\mathrm{d}}(\mathrm{j}\omega)}{\mathbf{I}_{\mathrm{d}}(\mathrm{j}\omega)} \tag{11}$$

III. Experimental Results

A. Measured grid impedance

Fig. 9 shows the measured grid impedance d-component with three different grid inductance values. The black curve shows the grid impedance which is affected only by the isolation transformer and the actual grid impedance seen at the interconnection point. The blue and green curves show the measured impedance when additional inductance of 1.5 or 5 mH is added between the inverter and the transformer. The PRBS-method is found to give accurate estimation on the grid impedance. The dotted lines represent the analytical grid impedance. By theory, the measurement is accurate up to one third of the sampling frequency, i.e., up to roughly 830 Hz [18]. However, the magnitude curve seems to follow the analytical grid impedance accurately up to 2 kHz.

The analytical model of the grid impedance is assumed as $Z_{\text{dd-grid}} = 1 + s \cdot 1.7 \cdot 10^{-3} + sL_2$, where L_2 is the value of the extra series-inductance. The isolation transformer and the grid was measured to have a total inductance of 1.7 mH which is represented as L_{g} in Fig. 1. Moreover, the total equivalent resistance of the transformer and the grid was measured to be approximately 1 ohm, corresponding to R_{g} in Fig. 1.

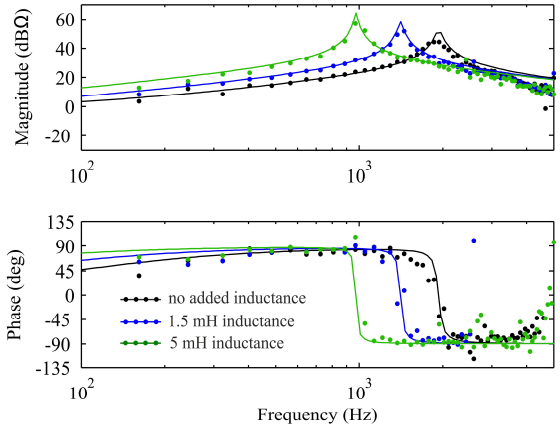

Fig. 9: Identified grid impedance with different values of grid-side inductance.

One of the main challenges is to cover a wide enough bandwidth with sufficient accuracy. The maximum generating frequency is limited by the inverter switching frequency (10 kHz). However, the current and voltage should be sampled at 2 to 4 times smaller frequency to increase accuracy which limits the achievable bandwidth.

The measurement accuracy can be improved by several methods. Assuming the injection amplitude cannot be increased, the simplest method would be increasing the number of injection periods and applying averaging. Using P excitation periods the effect of noise is reduced by $1/\sqrt{P}$. Another technique is to apply different injection type such as discrete-interval binary sequence (DIBS). The DIBS is a computer-optimized signal where certain number of harmonic frequencies are specified from a binary sequence, and their energy is maximized at the cost of non specified harmonic frequencies (without increasing the signal time-domain amplitude). The DIBS was applied for three-phase grid impedance measurement in [13].

B. Harmonic resonance

Figs. 10 and 11 show the grid current waveforms in stable and unstable case when an additional 6.5 mH inductance is

added. The MLBS injection is deactivated during the first experiment to illustrate the harmonic resonance phenomenon. In the first case (Fig. 10) the proportional feedforward gain K_{ff} is selected as 50 percent of the nominal value. The grid current includes fifth harmonic due to background harmonics and the fact that harmonic compensators are not used. However, the grid currents are stable.

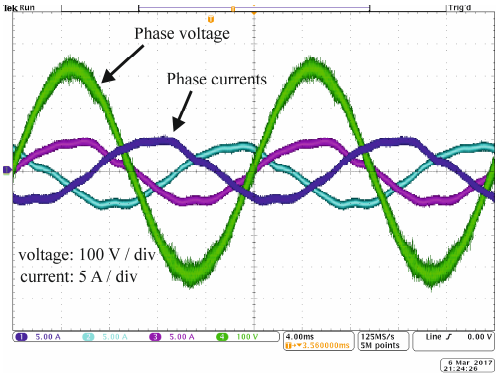

Fig. 10: Grid waveforms when feedforward gain is 50 % of the nominal value.

Fig. 11 shows the grid currents and one phase voltage in the unstable case. The inverter becomes unstable when the proportional feedforward gain is increased near to its optimal value of 100%. The resonance is caused by a lack of impedance-based stability margin, i.e., a harmonic resonance. The time-domain waveforms resemble to harmonic resonance which has been reported in [1].

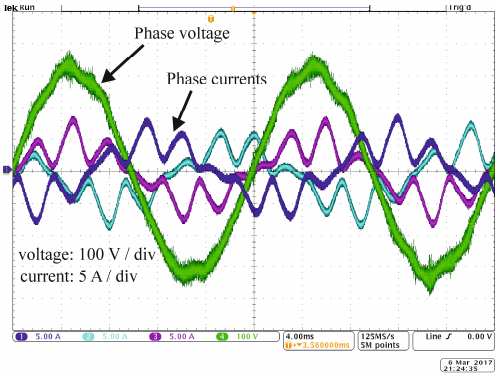

Fig. 11: Grid waveforms when feedforward gain is equal to the nominal value and inverter is unstable.

Fig. 12 shows the frequency spectrum of grid current during the instability. The spikes in the spectrum are not located at the harmonic frequencies and, thus, are not caused by background distortion of grid voltage or dead-time effect. The resonance can be explained by analyzing the ratio of grid and inverter impedances. A harmonic resonance is usually characterized by two spikes in the frequency spectrum which are located twice the fundamental frequency apart from each other.

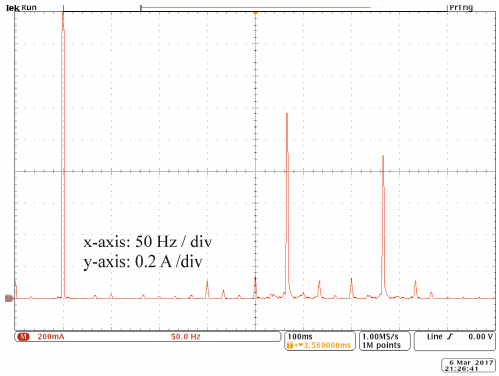

Fig. 12: Spectrum of grid current during the harmonic resonance.

Fig. 13 shows the measured grid impedance in green and inverter impedance (extracted from simulator) in blue. The impedances overlap at approximately 430 Hz with a phase difference more than 180 degrees which indicates a lack of stability margin. The main reason for instability is the fact that proportional feedforward decreases the phase of inverter impedance below -90 degrees due to control delay. Therefore, the inverter can become unstable even in the case of passive grid impedance.

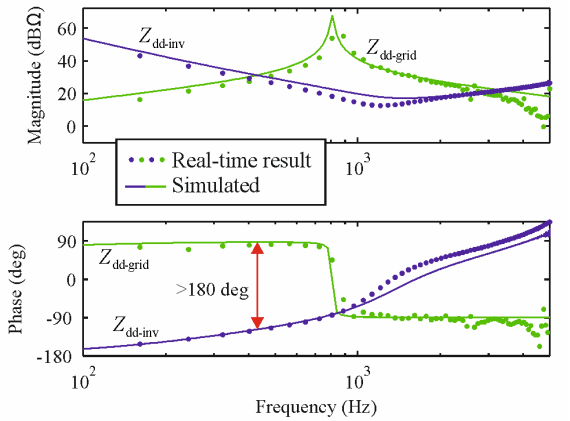

Fig. 13: Impedance d-components in the unstable case.

C. *Real-time stability analysis*

Fig. 14 shows the ratio of grid and inverter impedance when the proportional feedforward gain has values of 100, 80 and 50 percent of the nominal value. The ratio is plotted on complex-plane and is often also called as the Nyquist –contour. According to Nyquist stability criterion a system is unstable if the contour encircles the -1,0 point. In fact, the contour suggests instability when feedforward gain is increased close to the nominal value. Only the positive frequencies are shown to improve readability of the figures.

The Nyquist-contours are recorded from the dSPACE control platform while the inverter is online and subsequently plotted using MATLAB. A video is available online which shows how the contours look like in the actual implementation [19]. The online stability analysis tool is implemented using the Control Desk software since it allows seamless data transfer between a PC and dSPACE platform.

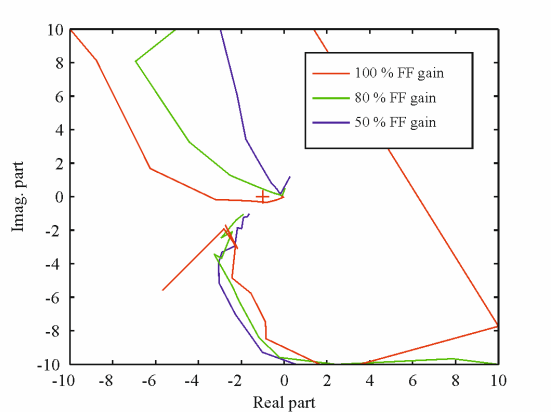

Fig. 14: Nyquist-contours based on online grid impedance identification (FF:feedforward).

A screen capture of the real-time stability assessment user interface is shown in Fig. 15. The upper left hand side shows the measured grid impedance and the computed inverter impedance. The corresponding Nyquist –contour is shown in the upper part of the right hand side. Grid currents are shown at the bottom right for monitoring purposes. Three sliders on the bottom provide access to MLBS amplitude, grid current reference and proportional grid voltage feedforward gain. The sliders can be used to change control parameters online to cause impedance-based interactions and to visualize stability margin in real-time.

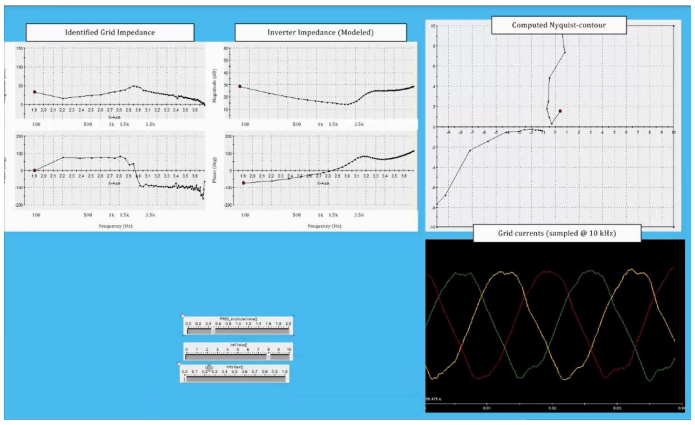

Fig. 15: User interface of the online stability monitoring tool implemented using Control Desk.

Fig. 16 shows the grid current when the grid impedance measurement is activated (in stable case). The MLBS amplitude is 0.5 A. It should be noted that the MLBS signal does degrade the power quality. However, its energy is divided over several different frequencies and it is not located at a single harmonic. This work does not consider minimizing the effect of MLBS on the power quality and it is suggested as a future topic. However, the amplitude of the MLBS signal can be decreased by using more periods as discussed above. In the proposed method, 20 MLBS periods were used to compute the grid impedance. This was found out to be the maximum limit before the control platform experienced an overrun and halted.

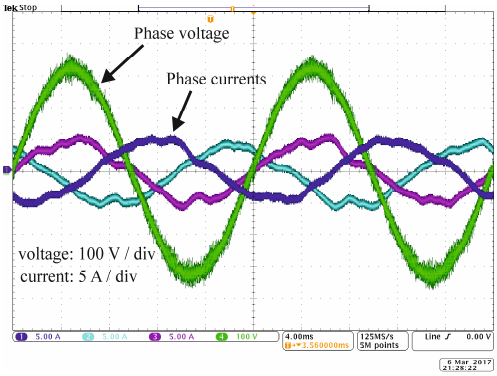

Fig. 16: Grid currents when the grid impedance identification is active.

IV. Discussion and Future Work

It has been demonstrated in this paper that a grid-connected inverter can be used to monitor the impedance-based stability margin based on the identified grid impedance. This section discusses some of the future possibilities and limitations of such technique.

Accuracy of stability analysis:

The measured impedance can be used to plot the ratio of inverter and grid impedance in real-time to allow online monitoring of stability margin. However, the accuracy depends greatly on the amount of simplification made regarding the stability criterion and the inverter impedance model. For most accurate stability analysis the full-order impedance model should be used to compute the inverter impedance. Thus, all eight impedance components (1) and (2) should be used in the stability analysis as discussed in [14]. Moreover, the method could be applied using sequence-impedances to improvethe accuracy.

Accuracy of impedance measurement:

The accuracy of the measured grid impedance is dependent on many factors, such as generating and sampling frequencies of the MLBS signal. However, the maximum generating frequency is limited by the switching frequency of the power converter. By theory, the accuracy of the measurement starts to degrade beyond one-third of the sampling frequency. Therefore, measuring grid impedance accurately in the range of several kilohertz would require more averaging and possibly larger perturbation amplitude. Moreover, the grid synchronization affects the measured grid impedance q-component at low frequencies which may become an issue if the converter utilizes a high-bandwidth PLL.

Adaptive control:

The paper has demonstrated that the method can extract the Nyquist contour which includes information about the impedance-based stability margin. The next logical step would be to transform this data into something more useful, such as a numerical value of the phase margin. The phase margin could then be used as an input for an adaptive control algorithm which shapes the inverter impedance in real-time to maintain a fixed stability margin.

Post-fault monitoring:

The method would allow extensive post-fault diagnostics if the grid impedance is recorded before a fault or disconnection occurs. One of the challenges is the randomness of these events, which means that the measurement should be active all the time and, thus, power quality should be considered very carefully.

Turn-on diagnostics:

The method could be used as a part of turn-on self-diagnostics to check the stability margin before the inverter starts to feed power into the grid. Measuring the grid impedance does not require a large fundamental component to be injected. Therefore, suitable control parameters could be selected to maintain stable operation, before the inverter starts feeding power.

V. Conclusions

In this work PRBS signal injection method is applied to measure the grid impedance online and to enable a visual real-time assessment of impedance-based stability in a grid-connected inverter. A PRBS-signal is injected to output currents of a grid-connected inverter to enable online grid impedance measurement. The measured grid impedance is used to plot the impedance ratio at the interface between inverter and the grid by utilizing an analytical model of inverter impedance. The Nyquist contour is plotted in real-time, allowing online visual assessment of stability margin.

The real-time analysis of stability margin provides many potential benefits: The method can be used as part of a start-up routine to estimate stability margin before activating control functions, such as reactive power control or grid voltage feedforward. Moreover, the method can be used for fault diagnostics after a disconnection in order to determine if the cause for tripping was a lack of stability margin. This, of course, requires Nyquist contours to be recorded continuously before the fault within a suitable time-window. Finally, the method provides an attractive basis for an adaptive control algorithms.

Acknowledgment

This research could not have been possible without the possibility for research visit in Aalborg University hosted by Professor Frede Blaabjerg. Moreover, funding provided by the Academy of Finland is highly appreciated.

Appendix

The MATLAB code to solve open-loop transfer functions can be given as follows:

```
% Open-loop transfer functions of voltage-fed inverter
run parameters %parameters defined in another file
s=tf('s');
A=[-r_eq/L, omega; -omega, -r_eq/L];
B=[Dd/L, -1/L, 0, Vin/L, 0; Dq/L, 0, -1/L, 0, Vin/L];
C=[3*Dd/2, 3*Dq/2; 1, 0; 0, 1];
D=[0, 0, 0, 3*ILd/2, 3*ILq/2; 0, 0, 0, 0, 0; 0, 0, 0, 0, 0];
G=C*(inv(s*eye(2)-A)*B)+D;

%input dynamics at open-loop
Yin_o=G(1,1);Toid_o=G(1,2), Toid_o=G(1,3);
Gcid_o=G(1,4), Gciq_o=G(1,5);

%open-loop output dynamics (d-channel)
Giod_o=G(2,1);Yodd_o=-G(2,2), Yoqd_o=-G(2,3);
Gcodd_o=G(2,4), Gcoqd_o=G(2,5);

%open-loop output dynamics (q-channel)
Gioq_o=G(3,1);Yodq_o=-G(3,2), Yoqq_o=-G(3,3);
Gcodq_o=G(3,4), Gcoqq_o=G(3,5);
```

References

[1] C. Li, "Unstable Operation of Photovoltaic Inverter from Field Experiences," *IEEE Trans. Power Deliv.*, vol. 8977, no. c, pp. 1–1, 2017.

[2] P. Belkin, "Event of 10/22/09," *CREZ Tech. Conf. Electr. Reliab. Counc. TExas*, 2010.

[3] J. Sun, "Impedance-based stability criterion for grid-connected inverters," *IEEE Trans. Power Electron.*, vol. 26, no. 11, pp. 3075–3078, 2011.

[4] L. Harnefors, X. Wang, A. Yepes, and F. Blaabjerg, "Passivity-Based Stability Assessment of Grid-Connected VSCs - An Overview," *IEEE J. Emerg. Sel. Top. Power Electron.*, vol. 4, no. 1, pp. 116–125, 2015.

[5] L. Jessen and F. W. Fuchs, "Modeling of inverter output impedance for stability analysis in combination with measured grid impedances," in *2015 IEEE 6th International Symposium on Power Electronics for Distributed Generation Systems (PEDG)*, 2015, pp. 1–7.

[6] T. Messo, J. Jokipii, A. Mäkinen, and T. Suntio, "Modeling the Grid Synchronization Induced Negative-Resistor-Like Behavior in the Output Impedance of a Three-Phase Photovoltaic Inverter," *4th IEEE Int. Symp. Power Electron. Distrib. Gener. Syst.*, pp. 1–7, 2013.

[7] B. Wen, D. Boroyevich, R. Burgos, P. Mattavelli, and Z. Shen, "Analysis of D-Q Small-Signal Impedance of Grid-Tied Inverters," *IEEE Trans. Power Electron.*, vol. 31, no. 1, pp. 675–687, Jan. 2016.

[8] T. Messo, J. Jokipii, A. Aapro, and T. Suntio, "Time and frequency-domain evidence on power quality issues caused by grid-connected three-phase photovoltaic inverters," *2014 16th Eur. Conf. Power Electron. Appl. EPE-ECCE Eur. 2014*, 2014.

[9] A. Rygg and M. Molinas, "Real-time stability analysis of power electronic systems," in *2016 IEEE 17th Workshop on Control and Modeling for Power Electronics (COMPEL)*, 2016, pp. 1–7.

[10] M. Cespedes and J. Sun, "Adaptive Control of Grid-Connected Inverters Based on Online Grid Impedance Measurements," *IEEE Trans. Sustain. Energy*, vol. 5, no. 2, pp. 516–523, Apr. 2014.

[11] T. Roinila, R. Luhtala, T. Reinikka, T. Messo, A. Aapro, and J. Sihvo, "dSPACE implementation for real-time stability analysis of three-phase grid-connected systems applying MLBS injection," *9th EUROSIM Congr. Model. Simul.*, pp. 1–6, 2016.

[12] T. T. Do, M. Jordan, H. Langkowski, and D. Schulz, "Novel grid impedance measurement setups in electrical power systems," in *2016 IEEE International Workshop on Applied Measurements for Power Systems (AMPS)*, 2016, pp. 1–6.

[13] T. Roinila, M. Vilkko, and J. Sun, "Online grid impedance measurement using discrete-interval binary sequence injection," *IEEE J. Emerg. Sel. Top. Power Electron.*, vol. 2, no. 4, pp. 985–993, 2014.

[14] T. Messo, A. Aapro, and T. Suntio, "Generalized multivariable small-signal model of three-phase grid-connected inverter in DQ-Domain," *IEEE 16th Work. Control Model. Power Electron.*, pp. 1–8, 2015.

[15] T. Roinila, T. Messo, and A. Aapro, "Impedance measurement of three phase systems in DQ-domain: Applying MIMO-identification techniques," in *2016 IEEE Energy Conversion Congress and Exposition (ECCE)*, 2016, pp. 1–6.

[16] T. Messo, A. Aapro, T. Suntio, and T. Roinila, "Design of grid-voltage feedforward to increase impedance of grid-connected three-phase inverters with LCL-filter," in *2016 IEEE 8th International Power Electronics and Motion Control Conference (IPEMC-ECCE Asia)*, 2016, pp. 2675–2682.

[17] T. Suntio, T. Messo, and J. Puukko, (forthcoming), *Power Electronic Converters: Dynamics and Control in Conventional and Renewable Energy Applications*, John Wiley & Sons Ltd., Chichester.

[18] T. Roinila, M. Vilkko, and J. Sun, "Broadband methods for online grid impedance measurement," in *2013 IEEE Energy Conversion Congress and Exposition*, 2013, pp. 3003–3010.

[19] T. Messo and D. Yang, "Real-Time Impedance-Based Stability Assessment of Grid Converter Interactions," *Youtube*, 2017. [Online]. Available: https://youtu.be/r65ZMg988f0.